Universitat Politècnica de Catalunya (UPC)
Universitat Autònoma de Barcelona (UAB)
Universitat de Barcelona (UB)
Institut de Ciències Fotòniques (ICFO)

http://www.photonicsbcn.eu

Master in Photonics

MASTER THESIS WORK

Point and shoot microvibrometry for biological applications

Alexandre de Matos Gomes Belsley

Supervised by Prof. Santiago Royo, CD6

Presented on the 8th of September, 2017

Registered at

Escola Tècnica Superior d'Enginyeria de Telecomunicació de Barcelona

Point and shoot microvibrometry for biological applications

Alexandre de Matos Gomes Belsley

Centre for Sensors, Instruments and Systems Development (CD6)
Rambla de Sant Nebridi, 10, 08222 Terrassa, Barcelona, Spain

E-mail: alexmgbelsley@gmail.com

September 2017

Abstract. The capabilities of an experimental setup combining the functions of a conventional microscope with a custom built self-mixing interferometer to characterize the contractile motion of living cells in both the transversal and longitudinal directions were explored. The use of discrete wavelets to denoise experimental signals combined with the application of a Hampel filter was shown to outperform standard denoising methods found in the self-mixing literature. Furthermore, an efficient iterative method to reliably estimate the optical feedback level and the linewidth enhancement factor was developed. Experimental displacements of microspheres, used as phantoms for living cells, were reconstructed with a resolution better than 0.15λ using the proposed reconstruction method. These results substantiate the claim that the proposed reconstruction method will enable the measurement of the contractile motion of individual cardiomyocytes with a resolution approaching 100 nm.

1. Introduction

The mechanical properties of biological cells are an important indicator of their state of health. The work described in this thesis represents initial steps towards developing the capabilities to measure the surface movement of biological cells through non-contact methods with a resolution approaching 100 nm. Previous works on self-mixing interferometry have shown that it is a suitable noninvasive optical technique for both *in vivo* and *ex vivo* biosensing [1]. A particular aim of the group within which this project was carried out is the study of the contractile motion of cardiomyocytes. The strength of contraction of cardiac cells is one of the first properties that deteriorates when the cells are subjected to specific pathologies [2].

Cardiomyocytes are cylindrical cells with a longitudinal axis approximately 100 µm long and a transverse diameter of 10-25 µm that, when excited by an electrical signal, move transversally and longitudinally. Video microscopy for monitoring the motion of cells within the focal plane (xy plane in figure 1) is a well-established method. However, some theoretical models predict that the displacement of the cells along the z direction can be important to identify certain pathologies [3].

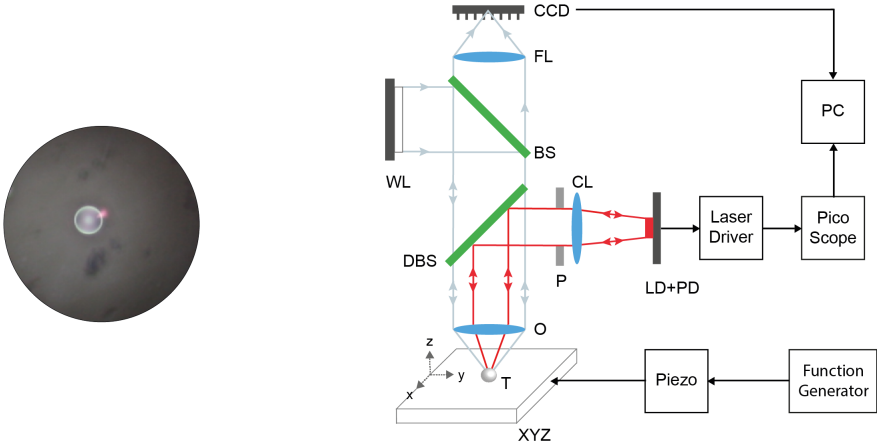

Figure 1: Photograph of a glass microsphere captured by the CCD with the visible laser red spot (left). Experimental setup. LD+PD: laser diode with integrated photodiode; WL: white light source; CL: collimating lens; FL: focusing lens; O: objective lens; P: pinhole; DBS: dichroic beam splitter; BS: 50/50 beam splitter; T: target; XYZ: xyz translation stage (right).

To measure all displacement components of the cells, the experimental setup shown in figure 1 was developed by the host group. This setup combines the functions of a conventional microscope equipped with an imaging CCD together with a custom-built self-mixing interferometer that measures sub-micrometer displacements along the z direction. The beam emitted by a Thorlabs HL8338MG 830 nm diode laser, after passing through a collimating lens, a pinhole with a variable diameter of 500-1000 µm, a beam splitter and an objective lens with a numerical aperture of 0.55, impinges on the target. A Canon EOS 1000D camera is used together with a white light source to adjust the target's position to lie in the focal plane of the incident laser beam using a xyz translation stage with micrometer precision. Since at this point of the project viable cardiomyocytes were not available, Merck Glass spheres with diameters ranging from 9-13 µm were used as phantoms to represent the cardiac cells as they have a similar size. The spheres were vertically displaced in a controlled manner by a E-665 Physik Instrumente piezoelectric transducer connected to a Tektronix AFG3102 function generator. A PicoScope 2208 oscilloscope connected to a PC was used to register the self-mixing signals (SMSs).

1.1. Basics of Self Mixing Interferometry (SMI)

When the laser beam impinges on the moving target at a distance $d(t)$ from the laser diode, a small part of the radiation is backscattered by the target into the laser cavity. This leads to a mixing between the original laser beam and the backscattered beam, and to a modulation of the power $P(t)$ emitted by the laser, which is given by [4]

$$P(t) = P_0[1 + m_A \cos(\phi_F(t))] \tag{1}$$

where P_0 is the power emitted by the free running laser, m_A is the amplitude modulation index and $\phi_F(t) = \frac{4\pi}{\lambda_F} d(t)$ is the external round-trip phase at the perturbed laser wavelength λ_F. $P(t)$ can be conveniently monitored using the built-in photodiode in the laser package, making the setup a self-aligned, extremely compact interferometer. Typically the DC component P_0 is filtered out, leaving what is conventionally known as the self-mixing signal (SMS) which is linearly proportional to $\cos(\phi_F(t))$ [5].

In the presence of optical feedback, the wavelength λ_F emitted by the laser is no longer constant. It can be determined by solving the excess phase equation [4]

$$\phi_0(t) = \phi_F(t) + C \sin[\phi_F(t) + \text{atan}(\alpha)] \tag{2}$$

where α is the linewidth enhancement factor and

$$\phi_0(t) = \frac{4\pi}{\lambda_0} d(t) \tag{3}$$

is the external round-trip phase at the free-running laser wavelength λ_0. C is the optical feedback level whose value depends mainly on the reflectivity of the target and its distance from the laser. Depending on its value, we can specify two relevant regimes for sensing applications: the weak regime for $C \leq 1$ and the moderate regime for $1 < C < 4.6$ [4].

2. Signal Processing

2.1. Denoising

Accurate and efficient denoising is an essential first step to reconstruct the target's displacement. The experimental signals registered had much stronger components of both random noise and coherent spikes than typical SMSs. Standard SMS filtering techniques include the use of moving average filters to remove white noise and median filters to remove speckle noise [6].

This approach was found to be insufficient and more sophisticated signal processing techniques were explored. Large noise spikes which are frequent in experimental SMSs are particularly difficult to remove because of the relatively slow time scales associated with the acquisition electronics.

It was found that a Hampel filter was able to successfully identify and correct hundreds of outliers in the SMSs registered. Removing these outliers allows the translation invariant discrete wavelet transform (TIDWT) to be more efficient at matching the fringe frequencies. This procedure produced significantly higher signal to noise ratios (SNRs) than were obtained either from applying standard SMSs denoising techniques or from only applying the TIDWT. An additional final pass through a Hampel filter removes some residual outliers, slightly cleaning up the final denoised signal. To the best of our knowledge, neither Hampel filters nor the TIDWT have been previously

used to denoise SMSs. Numerical codes used to implement the TIDWT and the Hampel filter were based on [7] and [8].

To compare the performance of the different denoising methods discussed above, an ideal simulated SMS with $C = 0.5$ and $\alpha = 5$ corresponding to a sinusoidal target displacement with amplitude of 2.5 µm and frequency of 4 Hz was corrupted with additive white Gaussian noise (AWGN) with a standard deviation $\sigma = 1.0$, leading to an initial SNR = 0.39 dB. The denoised signals obtained and the corresponding SNRs are shown in figure 2. A notched box plot [9] of the residuals relative to the ideal normalized SMS for the various methods is shown in figure 3.

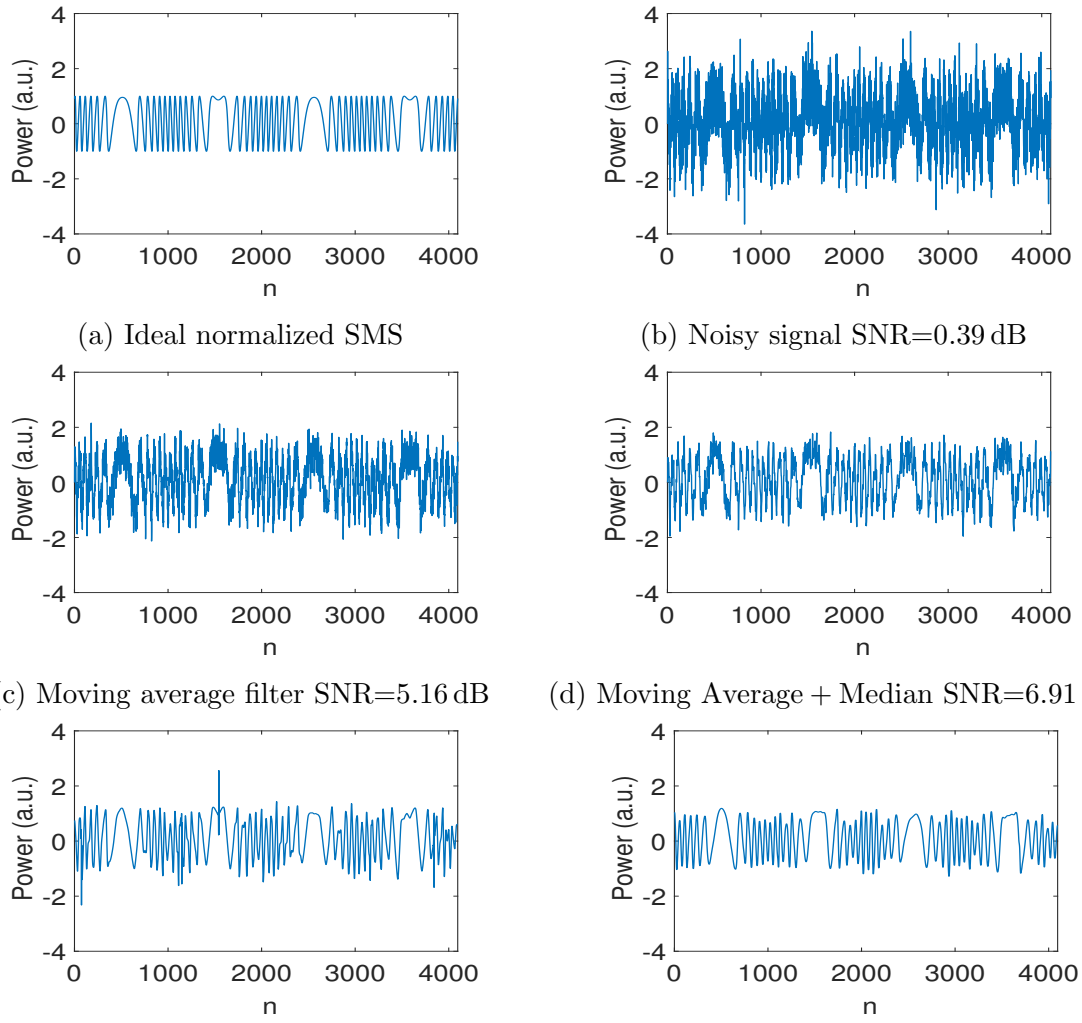

(a) Ideal normalized SMS

(b) Noisy signal SNR=0.39 dB

(c) Moving average filter SNR=5.16 dB

(d) Moving Average + Median SNR=6.91 dB

(e) TIDWT SNR=8.21 dB

(f) Hampel filters + TIDWT SNR=11.62 dB

Figure 2: SMS signal with noise applied and associated SNR values after the application of different denoising procedures; (a) Ideal (simulated) SMS, (b) Ideal SMS corrupted with AWGN with $\sigma = 1.0$; Denoised signals using (c) a moving average filter with a length $L = 3$; (d) a moving average filter with a length $L = 3$ and a median filter with length $L = 5$; (e) the TIDWT; and (f) one iteration of the Hampel filter, the TIDWT and a final iteration of the Hampel filter.

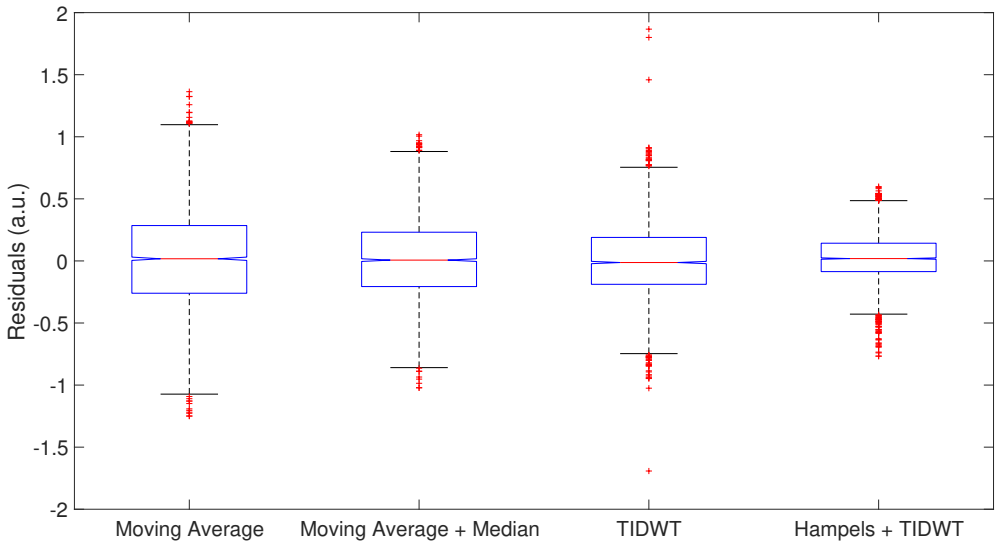

Figure 3: Notched box plot of the residuals between the ideal SMS and the denoised signal produced by the various denoising methods mentioned in the text.

From these figures we can see that the proposed denoising procedure has the highest SNR and a tighter distribution of residuals around zero. In fact, the spread between the 5% and 95% quartiles (represented by the upper and lower tick marks in figure 3) is almost a factor of two better than the standard method using the moving average filter. Furthermore, we can also see that the extent of the outliers surviving the TIDWT denoising procedure is greatly reduced by the use of the Hampel filter.

2.2. Phase Unwrapping Method

There are several ways of reconstructing the target displacement $d(t)$ from the SMS. The simplest method is based on the fact that each fringe corresponds to a target movement of $\lambda_0/2$. By counting the number of fringes, $d(t)$ can be easily obtained with an accuracy of $\lambda_0/2$ [5].

A more accurate alternative is the phase unwrapping method (PUM), where resolutions down to tens of nm have been reported [10]. In this method, ϕ_F is extracted from the SMS (see equation 1) and then the C and α parameters are estimated. Finally, ϕ_0 can be calculated from the nonlinear equation 2 and $d(t)$ can be directly retrieved from equation 3. The discussion of these steps below will be accompanied by the unwrapping of an experimental SMS obtained by displacing the spheres sinusoidally (a sinusoidal signal with 2 V peak to peak and 4 Hz was applied to the piezoelectric transducer).

2.2.1. Unwrapping ϕ_F

The first step is to obtain the wrapped version of ϕ_F by calculating the acos of the normalized SMS P_N, $\phi_{F_w} = acos(P_N)$.

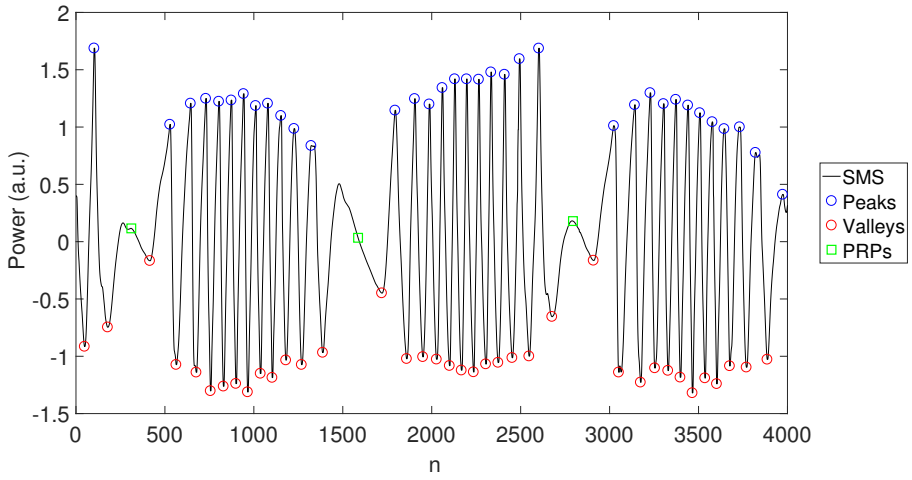

Figure 4: Salient features of the denoised SMS: peaks, valleys and phase reversal points. The SMS registered corresponded to a sinusoidal displacement of the microspheres.

An efficient method to normalize the SMS requires identifying several salient features, namely the peaks (maximum of each fringe), the valleys (minima of each fringe) and the phase reversal points (points where the movement of the target changes its direction).

The peaks and valleys of the signal were detected using a peakfinder function [11]. The usual way of detecting these extrema consists in calculating the derivative of the SMS and reshaping the differential signal to obtain a pulse train [12]. In the case of the signals measured, this approach was not robust enough, as many times it not only failed to identify all the required extrema but also resulted in the detection of spurious extrema due to the presence of noise spikes. The advantage of the peakfinder function is that it attempts to use the alternating nature of the derivatives along with two user defined thresholds to identify local extrema quickly and robustly.

The phase reversal points (PRPs) separate intervals in which the target is moving towards or away from the laser. Because of the nonlinearity in equation 2, the fringes are asymmetrical having a different shape for these two cases. For weak feedback ($C < 1$), the asymmetry is hardly noticeable as is the case in figure 4.

After extensive trials, it was found that the direction of travel could be determined by comparing the peak to valley ratio of the derivative of the SMS. In particular, when the target moves towards the laser the amplitude of the valleys of the SMS derivative are greater than the peaks and conversely when the target moves away from the laser.

To normalize the SMS an envelope function is created by fitting a cubic spline to the relevant extrema. The SMS is then divided by this envelope function to obtain a normalized signal. Due to the presence of noise, some extrema can extend slightly beyond ± 1. This can be handled by considering only the real part of the acos function when obtaining the wrapped phase ϕ_{F_w}.

In the next step, an accurate unwrapping of ϕ_F must take into account the phase

discontinuities that occur at the peaks and valleys of the SMS due to limited domain of the acos function (0 to π). These difficulties were solved by [12] who devised the following expression:

$$\phi_F(t) = (-1)^{(i_{V,P})}\phi_{F_W}(t) + 2\pi i_V \tag{4}$$

where $i_{V,P}$ is the total number of valleys and peaks that have occurred in the SMS up to time t and i_V is an index that increases by one for each ascending fringe valley and decreases by one for each descending fringe valley encountered until t.

2.2.2. C and α estimation

All the experimental signals measured belong to the weak feedback regime. In the literature one can find several methods to estimate C and/or α in this regime. A recently proposed method based on the Fourier transform of equation 2 [13] was implemented but we found it to give excessively large values with large dispersion for C with experimental (noisy) signals. Furthermore, the values obtained depended sensitively on the range of frequencies considered in the Fourier spectrum. This is a particularly difficult optimization problem for low feedback regimes and noisy signals, a quite common situation.

To obtain more robust estimates, a new procedure based on the previous work of [10] is proposed as part of the contributions of this thesis. The fundamental idea behind this optimization procedure is that the unwrapped phase should be a smooth curve except at possibly a small number of finite points. [10] implemented this by minimizing the sum of the derivative square of ϕ_0 over all time points. However, we found that much more reliable and robust results are achieved by minimizing the absolute value of the second derivative, i.e the curvature of ϕ_0. Furthermore it was found to be essential to use an efficient and robust numerical method to carry out the minimization procedure. To this end, a cyclic coordinate method based on a quadratic line search algorithm (adapted from [14]) was implemented to minimize the following cost function:

$$J(C,\alpha) = \sum_{t=0}^{T} \left| \frac{\partial^2 \phi_0(t;C,\alpha)}{\partial t^2} \right| \tag{5}$$

Independently of the initial guesses for C and α, the minimum of the cost function was reliably and quickly found as shown in table 1 for a wide range of simulated sinusoidal varying SMSs in the weak feedback regime, as appropriate for our experimental setup. It is worth pointing out that this method to estimate C and α can also be used in other feedback regimes. In the specific example of the experimental sinusoidal motion of the microspheres, a $C = 0.46$ and an $\alpha = 0.98$ were estimated.

It was also found through several simulations that the value of α has little effect on the accuracy of the displacement reconstruction for low values of feedback. This is in agreement with the findings in [15].

Table 1: Estimation of C and α with initial values $C = 0.5$ and $\alpha = 3$ on simulated SMSs. The difference between the true and estimated values of C and α as well as the number of iterations are also shown.

C_{true}	α_{true}	$C_{estim.}$	$\lvert C_{true} - C_{estim.} \rvert$	$\alpha_{estim.}$	$\lvert \alpha_{true} - \alpha_{estim.} \rvert$	# Iterations
0.200	2	0.201	0.001	1.969	0.031	12
	4	0.200	0	4.056	0.056	6
	6	0.200	0	6.137	0.137	14
0.600	2	0.600	0	1.992	0.008	6
	4	0.600	0	3.984	0.016	6
	6	0.600	0	5.975	0.025	6
1.000	2	1.000	0	1.998	0.002	6
	4	1.000	0	3.999	0.001	6
	6	1.000	0	5.999	0.001	4

2.2.3. Displacement reconstruction

Once $\phi_0(t)$ has been calculated, $d(t)$ is obtained directly from equation 3. In our particular example, the sinusoidal motion of the target was reconstructed with an accuracy of $0.086\lambda_0 \approx 71\,\text{nm}$ (see figure 5). Several sinusoidal and triangular displacements of the spheres with amplitudes between 5-7.5 µm and frequencies in the range of 4-10 Hz were reconstructed with an accuracy better than $\lambda_0/10$ (see table 2).

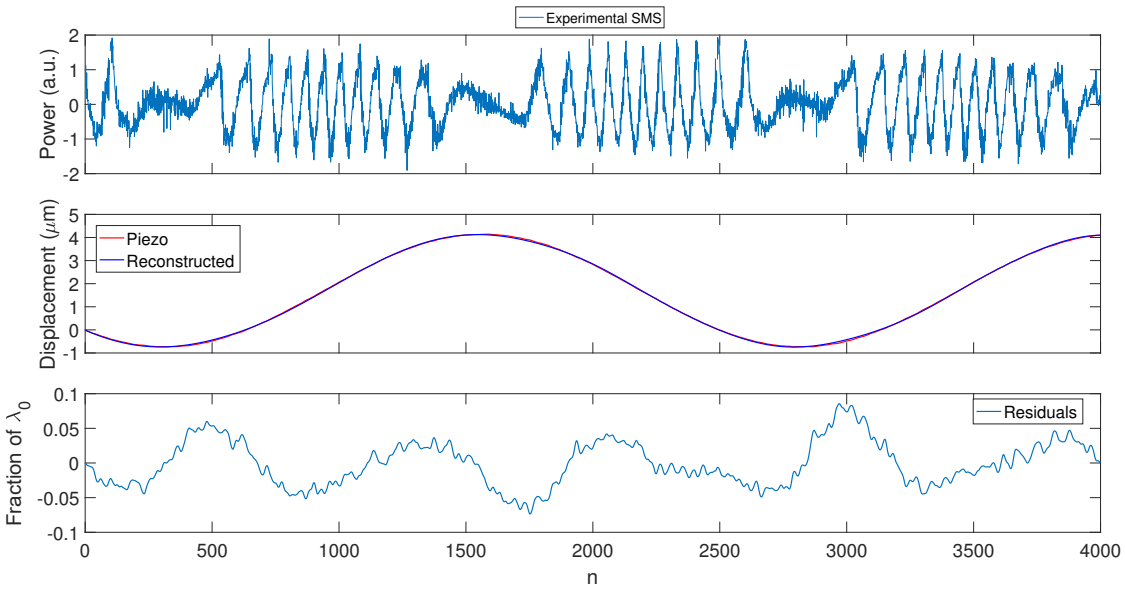

Figure 5: Experimental SMS corresponding to a sinusoidal motion undertaken by the spheres (top). Reconstructed displacement and piezo motion (middle). Residual errors between the reconstructed displacement and the piezo motion (bottom).

Table 2: Reconstruction error (maximum and standard deviation) of selected examples of experimental SMSs. The waveforms were varied and the frequencies and amplitudes selected to represent typical ranges expected for the contractile motion of cardiomyocytes. The optical feedback level $C_{estim.}$ estimated in each case is also shown.

Waveform	Frequency (Hz)	Amplitude (µm)	$\text{Error}_{\max}$(nm)	σ(nm)	$C_{estim.}$
Sine	4	5.0	$0.086\lambda_0 \approx 71$	27	0.46
Sine	10	5.0	$0.076\lambda_0 \approx 63$	25	0.51
Triangle	5	5.0	$0.084\lambda_0 \approx 70$	32	0.40
Triangle	5	7.5	$0.097\lambda_0 \approx 81$	48	0.43

3. Contractile motion of cardiomyocytes

In the first part of this work, the experimental SMSs acquired and reconstructed corresponded to symmetrical sinusoidal and triangular motions. To further test the efficacy of the PUM implemented, the microspheres were subject to a motion resembling the contractile motion of cardiomyocytes. Using the procedure described in the previous sections, a maximum reconstruction error of $0.15\lambda_0 \approx 125\,\text{nm}$ and a standard deviation $\sigma = \lambda_0/20 \approx 42\,\text{nm}$ were achieved (see figure 6). $C = 0.24$ and $\alpha = 1.7$ values were estimated.

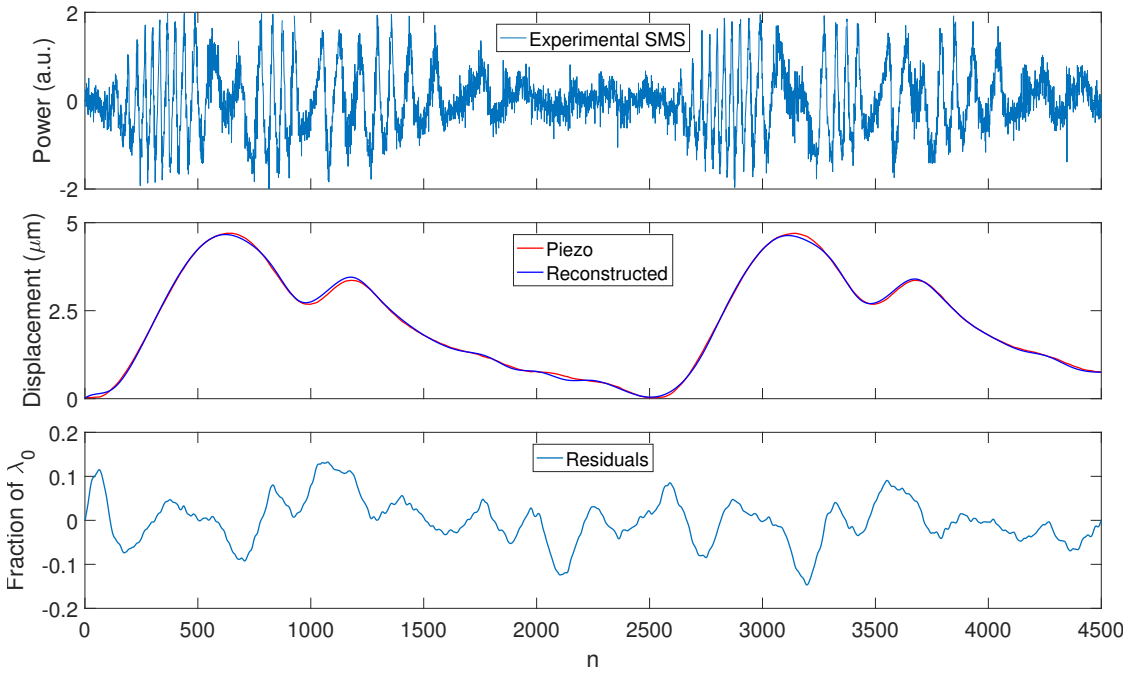

Figure 6: Experimental SMS corresponding to a motion resembling the contractile motion of cardiomyocytes undertaken by the spheres (top). Reconstructed displacement and piezo motion (middle). Residual errors between the reconstructed displacement and the piezo motion (bottom).

4. Conclusions

In this thesis work, a new setup to measure the displacement of microspheres along three orthogonal directions was explored. In comparison to typical SMSs, our signals had much stronger components of both random noise and coherent stochastic spikes. As a consequence, the denoising process is especially critical for our signals. To this end, a new denoising procedure combining an initial and final application of a Hampel filter with the TIDWT was proposed and it was shown that it had had a significantly better performance than other standard SMS denoising methods found in the literature.

Furthermore, in the PUM an accurate estimation of C is required. Different methods to estimate C and α proposed in the literature were tested but yielded unsatisfactory results given the above mentioned characteristics of our experimental signals. Hence a new robust and efficient method based on the minimization of the curvature of ϕ_0 was developed. It was able to very accurately estimate C and α for ideal SMSs with AWGN and also produced robust estimates for our experimental SMSs.

These improvements allowed the reconstruction of triangular and sinusoidal micrometer displacements of the microspheres with an accuracy better than $\lambda_0/10$. Additionally, the microspheres were used as phantoms to simulate the contractile motion of cardiomyocytes. Corresponding experimental SMSs were reconstructed with a maximum error of $0.15\lambda_0$.

The results and methods reported in this thesis permit one to have a high degree of confidence that accurate displacement reconstruction can be carried out for signals acquired using the developed setup. This paves the way for planned future measurements of the contractile motion of living biological cells which can provide important information for the detection of existing and new pathologies.

Acknowledgment I would like to thank Carlos Yáñez for many insightful discussions.

References

[1] Perchoux *et al.* 2016 *Sensors* **16** 694
[2] Yelamarty R *et al.* 1992 *American Journal of Physiology-Cell Physiology* **262** C980–C990
[3] Ma Z *et al.* 2014 *Biomaterials* **35** 1367–1377
[4] Donati S 2012 *Laser Photonics Review* **417** 393–417
[5] Taimre T *et al.* 2015 *Adv. Opt. Photon.* **7** 570–631
[6] Liu Z *et al.* 2016 *Optical Engineering* **55** 104102–104102
[7] Peyré G 2011 *IEEE Computing in Science and Engineering* **13** 94–97
[8] Pearson R 2005 *Mining Imperfect Data: Dealing with Contamination and Incomplete Records*
[9] MathWorks Notched URL `mathworks.com/help/symbolic/mupad_ref/notched.html`
[10] Bes C *et al.* 2006 *IEEE Transactions on Instrumentation and Measurement* **55** 1101–1105
[11] Yoder N 2011 Peakfinder URL `www.mathworks.com/matlabcentral/fileexchange/25500`
[12] Fan Y *et al.* 2010 *Proceedings of SPIE* **7855** 1–7
[13] Yu Y and Xi J 2013 *Optical Society of America* **38** 1781–1783
[14] McNames J 2006 Lectures in engineering data analysis & modeling URL `web.cecs.pdx.edu/~edam/`
[15] Yu Y *et al.* 2011 *Optical Society of America* **19** 277–279